בס"ד

Frequency Modulated Waveforms for Integrated Imaging and Communications

Chirp OFdm

Peter Vouras
U.S. Department of Defense, Washington, D.C. 20375

***Abstract*—Combining the functions of environmental imaging and communication requires waveforms that are simultaneously modulated to convey information while retaining desirable detection properties such as low autocorrelation sidelobes. This paper explores the use of an optimized frequency modulated (FM) chirp waveform designed for integrated imaging and communications. The waveform is radiated by a moving transmitter, such as a synthetic aperture radar (SAR) mounted on an airborne or satellite platform, and it simultaneously embeds a communication bit stream while retaining the autocorrelation properties desired for creating images of a ground scene. The transmitted chirp contains spectral nulls within its bandwidth that are created by applying a continuous offset to the phase modulation function. Within the nulled spectral regions, a second waveform modulated by a communication bit stream can be inserted. Simulated results demonstrate two techniques for creating the spectral nulls in the adapted chirp.**

***Index Terms*—imaging and communications, spectral nulling**

I. Introduction

Integrated imaging and communications is an ambitious requirement that if implemented enhances the utility of conventional wireless platforms such as SAR or cell devices. Unfortunately, the objectives of imaging the environment while transmitting information are often not compatible. Transmitting information at high data rates requires complex signal modulations, such as Orthogonal Frequency Division Multiplexing (OFDM). These modulations in turn degrade the signal's detection properties that are necessary to maintain adequate environmental imaging or sensing performance. For example, the OFDM waveform has intrinsically high autocorrelation sidelobes that make it ill-suited for sensing weak objects in the environment. The authors in [1] describe a multiple input multiple output (MIMO) system that leverages a combined OFDM and Frequency Modulated Continuous Wave (FMCW) waveform. Other authors have also explored the use of an overlapping FMCW waveform for sensing purposes and an OFDM waveform for communication [2]. Radar and communication systems utilizing OFDM in the same bandwidth are described in [3]. The approach taken in [4] is to send the radar signal to the null space of the communication users. This paper proposes to adapt a chirp waveform by creating spectral nulls and within the nulled regions, inserting the subcarriers of an OFDM waveform. This framework mostly preserves the autocorrelation properties of the chirp while leveraging the bit-rate performance of OFDM.

II. Brief Overview of Existing Nulling Method

To begin, we briefly summarize the important steps of the existing method for creating spectral nulls in waveforms described by [5]. The method applies to a continuous-time pulse $s(t)$ of duration T with amplitude $a(t)$, phase modulation $\psi(t)$ and phase offset $\phi(t)$. The phase offset $\phi(t)$ is to be determined by the proposed nulling algorithm.

$$s(t) = a(t)e^{j(\psi(t)+\phi(t))} \tag{1}$$

For the case, of a linear frequency modulated (LFM) chirp, $\psi(t) \propto t^2$. The angular frequency spectrum of the pulse is given by,

$$S(\omega) = \frac{1}{T}\int_0^T a(t)e^{j(\psi(t)+\phi(t))}e^{-j\omega t}dt. \tag{2}$$

The objective of the nulling algorithm is to find a function $\phi(t)$ such that $S(\omega_k) = 0$ for $k = 1, \dots, K$ discrete frequencies. The phase offset $\phi(t)$ applied to the waveform $s(t)$ should be small, so the objective function becomes

$$\begin{aligned} &\min \quad ||\phi|| \\ &\text{such that} \quad S(\omega_k) = 0, \quad k = 1, \dots, K. \end{aligned} \tag{3}$$

Here, the norm and inner product are defined as

$$\begin{aligned} ||\phi|| &= \sqrt{\langle \phi, \phi \rangle}, \\ \langle g, h \rangle &= \frac{1}{T}\int_0^T g(t)h(t)dt. \end{aligned} \tag{4}$$

The approach taken in [5] to solve (1) is to replace the exact nonlinear constraints described by (3) with their linear first-order approximation as in [6],

$$\begin{aligned} &S(\omega_k; \phi(t) = 0) + \int_0^T \frac{\partial}{\partial \phi} S(\omega_k)\bigg|_{\phi=0} \phi(t)dt = 0, \\ &\text{for } k = 1, \dots, K. \end{aligned} \tag{5}$$

The result is a standard least-norm optimization problem

$$\begin{aligned} &\min \quad ||\phi|| \\ \text{תנאי אילוס} \quad &\text{such that} \quad \langle \mathbf{z}, \phi \rangle = j\langle \mathbf{z}, 1 \rangle \end{aligned} \tag{6}$$

where the vector $\mathbf{z}$ is defined as

$$\mathbf{z} = a(t)e^{j\psi(t)} \left[\begin{array}{ccc} e^{j\omega_1 t} & \dots & e^{j\omega_K t} \end{array} \right]. \tag{7}$$

2024 58th Asilomar Conference on Signals, Systems, and Computers | 979-8-3503-5405-8/24/$31.00 USG | DOI: 10.1109/IEEECONF60004.2024.10942641

The solution $\hat{\phi}(t)$ to (6) is given by [5],

$$\hat{\phi}(t) = \begin{bmatrix} \Re(\mathbf{z}) & \Im(\mathbf{z}) \end{bmatrix} \langle \begin{bmatrix} \Re(\mathbf{z}) & \Im(\mathbf{z}) \end{bmatrix}, \begin{bmatrix} \Re(\mathbf{z}) & \Im(\mathbf{z}) \end{bmatrix} \rangle^{-1} \times \langle \begin{bmatrix} -\Im(\mathbf{z}) & \Re(\mathbf{z}) \end{bmatrix}, 1 \rangle. \quad (8)$$

III. Null Depth Control Using Regularized Least Squares

To control the depth of a spectral null we seek the solution to the regularized least squares problem given by

$$X(\mathbf{f}) = \frac{1}{2}||\mathbf{y} - \mathbf{A}\mathbf{f}||^2 + \beta R(\mathbf{f})$$
$$\hat{\mathbf{f}} = \arg\min_{\mathbf{f}} X(\mathbf{f}) \quad (9)$$

The additive term $\beta R(\mathbf{f})$ in (9) with $\beta > 0$ is a regularization function or penalty that steers the program solution towards having desirable properties. For the problem at hand, if there are N time samples, we set

$$\mathbf{A} = \begin{bmatrix} \Re(\mathbf{z}) & \Im(\mathbf{z}) \end{bmatrix},$$
$$\mathbf{y} = \langle \begin{bmatrix} -\Im(\mathbf{z}) & \Re(\mathbf{z}) \end{bmatrix}, 1 \rangle,$$
$$\mathbf{f} = \begin{bmatrix} \phi(t_1) \\ \vdots \\ \phi(t_N) \end{bmatrix} \quad (10)$$

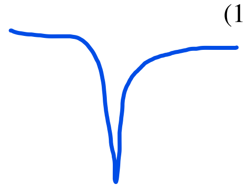

and use

$$R(\mathbf{f}) = \frac{1}{2}||\mathbf{D}\mathbf{f}||^2,$$
$$\mathbf{D} = \begin{bmatrix} 1 & -1 & 0 & \dots & 0 \\ 0 & 1 & -1 & \dots & 0 \\ \vdots & \ddots & \ddots & \vdots & \vdots \\ 0 & \dots & 0 & 1 & -1 \\ 0 & 0 & \dots & 0 & 1 \end{bmatrix}_{(N-1)\times N}. \quad (11)$$

The matrix-vector multiplication term $\mathbf{Df}$ computes successive differences between neighboring samples of the estimated phase offset function $\phi(t)$ [7]. Therefore, this choice of $R(\mathbf{f})$ limits the total variation or frequency excursion induced by $\phi(t)$ which will have the effect of controlling the null depth.

The solution to (9) can be found by a few iterations of the conjugate gradient algorithm shown below [8]. The algorithm proceeds for M iterations and the initial estimate $\mathbf{f}_0$ for the phase offset function is given by the solution $\hat{\phi}(t)$ from (8). The algorithm requires a data weighting matrix $\mathbf{W}$ and an optional preconditioning matrix $\mathbf{M}$ to accelerate convergence.

IV. Null Width Control Using Derivative Constraints

A simple yet effective method to create wider spectral nulls is to place multiple point nulls close together. In this section we describe a second approach to affect null width that relies on constraining the first and second derivatives of $S(\omega)$ with

Algorithm 1 Null Depth Control Algorithm

Initialization: $\mathbf{r} = \mathbf{y} - \mathbf{A}\mathbf{f}_0$. For $n = 0, 1, 2, \dots, M$ do

1: $\mathbf{g}_{new} = \mathbf{A}^H \mathbf{W} \mathbf{r} - \beta \mathbf{D}^H \mathbf{D} \mathbf{f}_n$

2: $\gamma = \begin{cases} 0, & \text{first iteration} \\ \dfrac{\mathbf{g}_{new}^H \mathbf{M} \mathbf{g}_{new}}{\mathbf{g}_{old}^H \mathbf{M} \mathbf{g}_{old}}, & \text{otherwise} \end{cases}$

3: $\mathbf{d} = \mathbf{M}\mathbf{g}_{new} + \gamma \mathbf{d}$

4: $\mathbf{q} = \mathbf{A}\mathbf{d}$

5: $\alpha = \dfrac{\mathbf{d}^H \mathbf{g}_{new}}{\mathbf{q}^H \mathbf{W} \mathbf{q} + \beta \mathbf{d}^H \mathbf{D}^H \mathbf{D} \mathbf{d}}$

6: $\mathbf{f}_{n+1} = \mathbf{f}_n + \alpha \mathbf{d}$

7: $\mathbf{r} = \mathbf{r} - \alpha \mathbf{q}$

8: $\mathbf{g}_{old} = \mathbf{g}_{new}$.

respect to frequency to equal zero at the null locations ω_k. The optimization problem now becomes,

$$\begin{aligned} & \min \quad ||\phi|| \\ \text{such that} \quad & S(\omega_k) = 0, \\ & \frac{\partial}{\partial \omega} S(\omega_k) = 0, \\ & \frac{\partial^2}{\partial \omega^2} S(\omega_k) = 0, \quad k = 1, \dots, K. \end{aligned} \quad (12)$$

The desired derivatives are given by,

$$\left.\frac{\partial}{\partial \omega} S(\omega)\right|_{\omega=\omega_k} = \frac{j}{T} \int_0^T a(t) e^{j(\psi(t)+\phi(t))} t e^{j\omega t} dt,$$
$$\left.\frac{\partial^2}{\partial \omega^2} S(\omega)\right|_{\omega=\omega_k} = -\frac{1}{T} \int_0^T a(t) e^{j(\psi(t)+\phi(t))} t^2 e^{j\omega t} dt. \quad (13)$$

The new derivative constraints are linearized by retaining their first-order approximations similar to (5). Since the derivative constraints are set equal to zero, the multiplicative scalars j/T and $-1/T$ in (13) can be dropped.

The result is again a standard least-norm optimization problem with extended constraints as in,

$$\begin{aligned} & \min \quad ||\phi|| \\ & \text{such that } \langle \hat{\mathbf{z}}, \phi \rangle = j \langle \hat{\mathbf{z}}, 1 \rangle \end{aligned} \quad (14)$$

where the vector $\hat{\mathbf{z}}$ is defined as

$$\hat{\mathbf{z}} = \begin{bmatrix} \mathbf{z} \\ t\mathbf{z} \\ t^2\mathbf{z} \end{bmatrix}. \quad (15)$$

The solution $\hat{\phi}_2(t)$ to (15) is given by,

$$\hat{\phi}_2(t) = \begin{bmatrix} \Re(\hat{\mathbf{z}}) & \Im(\hat{\mathbf{z}}) \end{bmatrix} \langle \begin{bmatrix} \Re(\hat{\mathbf{z}}) & \Im(\hat{\mathbf{z}}) \end{bmatrix}, \begin{bmatrix} \Re(\hat{\mathbf{z}}) & \Im(\hat{\mathbf{z}}) \end{bmatrix} \rangle^{-1} \times \langle \begin{bmatrix} -\Im(\hat{\mathbf{z}}) & \Re(\hat{\mathbf{z}}) \end{bmatrix}, 1 \rangle. \quad (16)$$

V. Numerical Experiments

The results in this section illustrate nulls created in the spectrum of a baseline chirp waveform. The parameters of the baseline chirp are a duration of $T = 60$ μsec and bandwidth $B = 2$ MHz.

A. Single Point Null

To begin, we illustrate results for a single point null. The desired null is at a frequency of 0.4 MHz. Fig. 1 illustrates the baseband I and Q components of the chirp and the optimized phase offset function computed using (8). Fig. 2 shows the

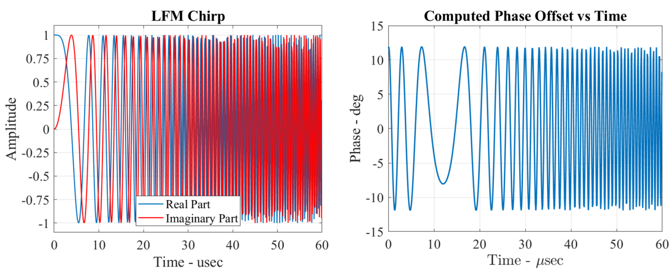

Fig. 1: (Left) Baseband I and Q components of chirp waveform. (Right) Computed phase offset function.

adapted chirp spectrum with a null placed at 0.4 MHz. The null has a depth of approximately -37 dB relative to the peak. Using the computed phase offset function shown in Fig. 1

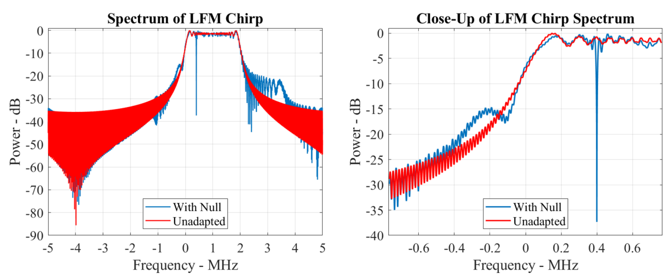

Fig. 2: (Left) Adapted chirp with spectral null at 0.4 MHz. (Right) Close-up view of null.

as the initial condition and proceeding with the iterations for Algorithm 1, yields the phase offset functions shown in Fig. 3 after 10 and 20 iterations. The algorithm parameters for this case are $\beta = 10,000$, $\mathbf{M} = \mathbf{I}$, and $\mathbf{W} = 4000\mathbf{I}$. The plots show that as the algorithm iterations increase, a taper is progressively applied to the estimated phase offset function. The resulting spectrum is shown in Fig. 4. As the plots show, the null depth is now approximately -12 dB below the peak. A second example of the output from Algorithm 1 is shown in Figs. 5 and 6. Once again, the computed phase offset function in Fig. 1 is used as the initial condition. The algorithm parameters for this case are $\beta = 1e6$, $\mathbf{M} = \mathbf{I}$, and $\mathbf{W} = 200\mathbf{I}$. The results show a null depth of approximately -22 dB and suggest that if a less severe taper is applied to the phase offset function then the null extends deeper.

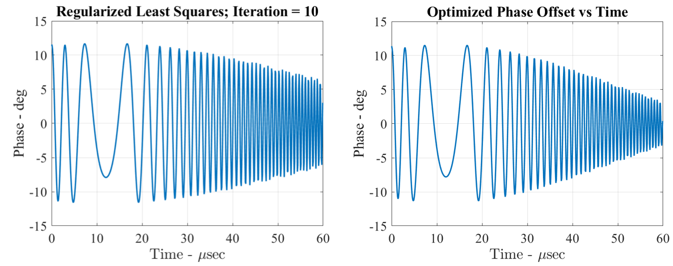

Fig. 3: (Left) Phase offset function after 10 iterations of Algorithm 1. (Right) Phase offset function after 20 iterations.

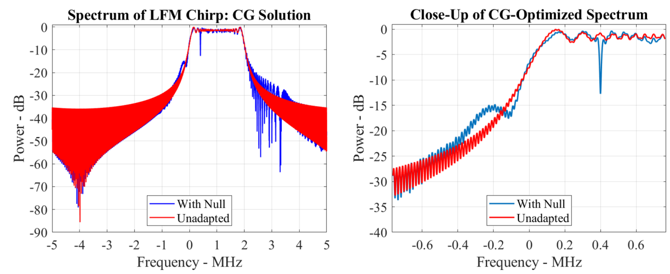

Fig. 4: Left) Adapted spectrum using Algorithm 1. (Right) Close-up view.

B. Multiple Nulls and the Case for Derivative Constraints

As previously suggested, placing multiple nulls close together can effectively widen the nulled region into a notch. Fig. 7 shows the results when 3 nulls are created at the frequencies $0.4, 0.415, 0.43$ MHz. The nulled region is clearly wider than the width of a single point null. Fig. 8 shows the matched filter output when the adapted chirp is convolved with an un-adapted chirp that does not have a phase offset function applied. The plot shows the sidelobes become slightly elevated and asymmetrical. The right side of Fig. 8 illustrates the phase offset function for 3 widely-spaced nulls at $0.2, 0.3, 0.4$ MHz. Fig. 9 illustrates the adapted spectrum for the case of 3 widely-spaced nulls. Fig. 10 shows the matched filter output for the case of 3 widely-spaced nulls when the adapted chirp is convolved with an un-adapted chirp. Also shown is the phase offset function computed using derivative constraints and the

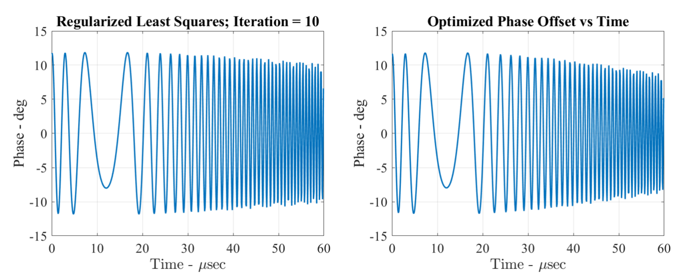

Fig. 5: (Left) Phase offset function after 10 iterations of Algorithm 1: Case 2. (Right) Phase offset function after 20 iterations.

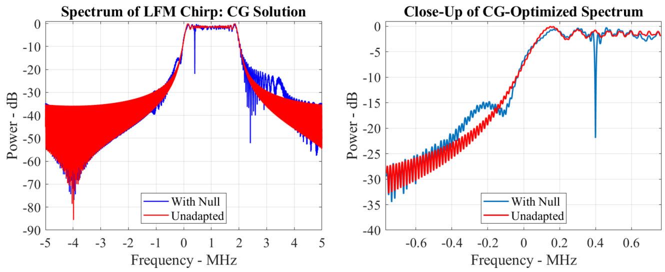

Fig. 6: (Left) Adapted spectrum using Algorithm 1: Case 2. (Right) Close-up view: Case 2.

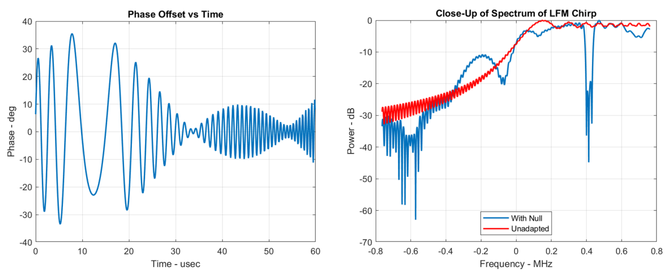

Fig. 7: (Left) Optimized phase function to create 3 closely-spaced nulls. (Right) Close-up view of adapted spectrum showing a wider notch.

solution from (16). Fig. 11 shows the resulting wider null and can be compared to Fig. 2.

VI. Conclusions

This paper describes the design of an optimized FM chirp waveform for integrated imaging and communications. The waveform is constructed by creating spectral nulls within the bandwidth of a traditional chirp. The nulls are generated by applying a continuous phase offset. Simulated results are presented to demonstrate techniques for controlling the depth and width of the desired nulls.

References

[1] H. K. Boddapati, K. K. Ashok, K. R. Chavva, M. S. Khan, "Joint Communication and Sensing for MIMO Systems with Overlapped OFDM and FMCW," *Proceedings of the 98th Vehicular Technology Conference*, Hong Kong, China, October 2023.

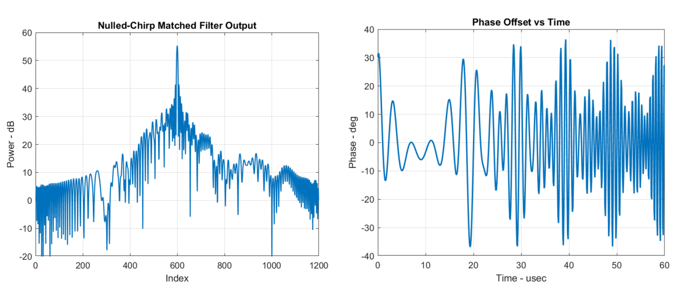

Fig. 8: (Left) Matched filter output for adapted chirp with 3 closely-spaced nulls. (Right) Phase offset function for 3 widely-spaced nulls.

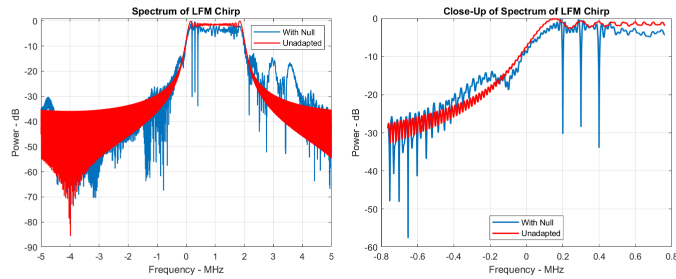

Fig. 9: (Left) Three widely-spaced nulls 0.1 MHz apart. (Right) Close-up view.

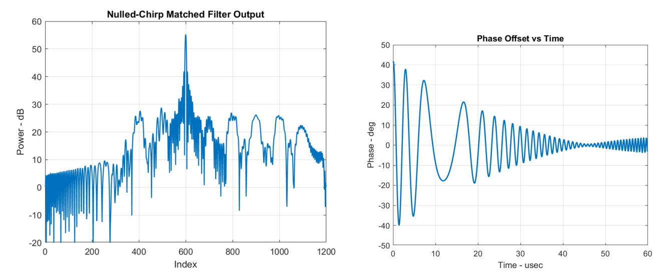

Fig. 10: (Left) Matched filter output for 3 widely-spaced nulls. (Right) Phase offset solution for derivative constraints.

[2] M. M. Sahin, H. Arslan, "Multi-Functional Coexistence of Radar Sensing and Communication Waveforms," *Proceedings of the 92nd Vehicular Technology Conference*, Victoria, BC, Canada, Feb. 2020.

[3] C. Shi, F. Wang, M. Sellathurai, J. Zhou, S. Salous, "Power Minimization-Based Robust OFDM Radar Waveform Design for Radar and Communication Systems in Coexistence," *IEEE Transactions on Signal Processing*, vol. 66, no. 5, pp. 1316–1330, November 2018.

[4] S. Sodagari, A. Khawar, T. C. Clancy, R. McGwier, "A Projection-Based Approach for Radar and Telecommunication Systems Coexistence," *Proceedings of the 2012 IEEE Global Communications Conference (GLOBECOM)*", Anaheim, CA, USA, pp. 5010–5014, December 2012.

[5] K. Gerlach, M. R. Frey, M. J. Steiner, A. Shackelford, "Spectral Nulling on Transmit via Nonlinear FM Radar Waveforms," *IEEE Trans. on Aerospace and Electronic Systems*, vol. 47, no. 2, pp. 1507–1515, April 2011.

[6] D. G. Luenberger, *Optimization by Vector Space Methods*, New York, NY: John Wiley and Sons, 1969.

[7] I. W. Selesnick, H. L. Graber, D. S. Pfeil, R. L. Barbour, "Simultaneous Low-Pass Filtering and Total Variation Denoising," *IEEE Trans. on Signal Processing*, vol. 62, no. 5, pp. 1109–1124, March 2014.

[8] B. P. Sutton, D. C. Noll, J. A. Fessler, "Fast, Iterative Image Reconstruction for MRI in the Presence of Field Inhomogeneities," *IEEE Trans. on Medical Imaging*, vol. 22, no. 2, pp. 178–188, February 2003.

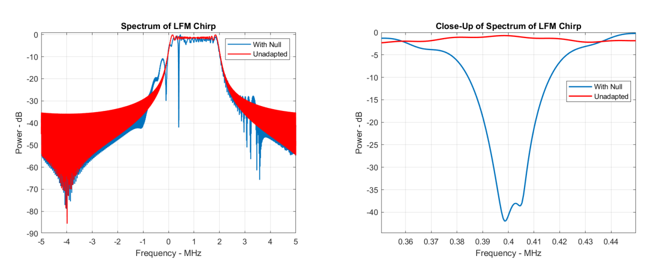

Fig. 11: (Left) Wider null computed using derivative constraints. (Right) Close-up view.